

Probing Molecular Mechanisms of Self-Assembly in Metal–Organic Frameworks

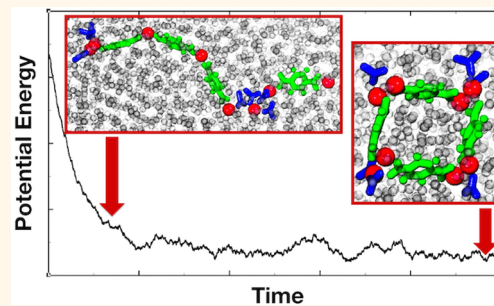
Debasmita Biswal and Peter G. Kusalik*

Department of Chemistry, University of Calgary, 2500 University Drive NW, Calgary, Alberta T2N 1N4, Canada

Supporting Information

ABSTRACT: Metal–organic framework materials (MOFs) are a class of nanoporous materials, important to many applications (e.g., gas storage, separation), and their synthesis has received considerable attention. Yet, very little is known about the mechanisms of self-assembly of MOFs. Here, we provide molecular-level insights into the previously unexplored behavior of the self-assembly process, through molecular dynamics simulations, for an archetypal Zn-carboxylate MOF system exhibiting complex vertex topologies (e.g., paddle-wheel clusters). A key finding of this study is the characterization of a stochastic and multistage ordering process intrinsic to self-assembly of the Zn-carboxylate MOF system. A variety of transient intermediate structures consisting of various types of Zn-ion clusters and carboxylate-ligand coordination, and featuring a range of geometric arrangements, are observed during structural evolution. The general features deduced here for the mechanism of the self-assembly of this archetypal MOF system expose the complexities of the various molecular-level events that can occur during the early stages of this process spanning time scales of nano- to microseconds. More generally, we provide fundamental insights that elucidate key aspects of the early stages of the self-assembly mechanism for an important class of nanoporous materials, and of experimental studies exploring nucleation and growth processes in such materials.

KEYWORDS: MOF self-assembly, molecular dynamics simulation, molecular-level mechanisms, multistage ordering, solvent dependence, Zn-carboxylate systems



Biological systems and natural minerals abound with examples of nanoporous materials that exhibit various interesting properties. For example, natural and synthetic zeolites have been regularly used as catalysts and adsorbents in industrial applications. Inspired by the efficiency of these naturally occurring materials, experimentalists have developed several design strategies and principles to synthesize nanoporous materials with tailored physicochemical properties. Metal–organic frameworks (MOF) or hybrid inorganic–organic materials represent an example of an important class of nanoporous crystalline materials^{1,2} significant to various applications.^{3–12} The numerous potential applications that MOFs offer have their origin in the precise control of the nanosized pore volume and have stimulated the design and synthesis of thousands of MOFs characterized by multifunctional properties. Despite the tremendous growth in the number of MOFs synthesized to date, the mechanism of MOF crystallization is poorly understood and a molecular-level description of MOF formation remains an open challenge. It is clearly important to understand the interactions between the constituent components and the physical factors governing the self-assembly processes involved¹³ in order to control structures and functionalities of MOFs. The aim of this study is to shed light on the underlying ordering processes, for example, kinetics

during the early stages of self-assembly, for an archetypal MOF comprising Zn-ions and carboxylate ligands.

Only a handful of experimental studies have directly explored formation processes of MOFs,^{13–19} where some have indicated that multiple intermediates^{13,14} can form during self-assembly. Nevertheless, the underlying molecular and mechanistic details (*i.e.*, the specifics of possible intermediate structures, the links between them, and questions of when they might appear) remain unclear. Moreover, the investigation of microscopic structures and molecular mechanisms of formation by direct experimental studies is very difficult. A detailed analysis of the self-assembly process in MOFs, as provided by molecular simulations, could in principle help reveal underlying mechanisms and offer significant insights into experimental observations.

There are very few theoretical studies^{20–24} performed to date exploring formation of MOFs, where only three of these have focused explicitly on self-assembly processes in periodic MOF and discrete metal–organic material systems. Yoneya *et al.*^{22–24} have reported the self-assembly of 2-D and 3-D periodic MOF structures composed of metal ions (Pd(II) and Ru(II)),

Received: August 12, 2016

Accepted: December 20, 2016

Published: December 20, 2016



ACS Publications

© XXXX American Chemical Society

A

DOI: 10.1021/acsnano.6b05444
ACS Nano XXXX, XXX, XXX–XXX

respectively) and neutral 4,4'-bipyridine ligands. Utilizing Langevin dynamics (LD) simulations and a continuum solvent model, these authors focused primarily on optimizing simulation parameters, such as tuning the solvent dielectric constant, to achieve formation of the corresponding discrete metal–organic material structure^{22,23} and periodic MOF structures.²⁴ Notably, these structures feature only single ion vertices. Given the important role that solvents play in self-assembly processes in experiments, it is unclear how the parametrized continuum solvent in these simulations might have impacted the observed behavior. It remains the case that even a basic understanding of the molecular processes underlying MOF self-assembly is currently lacking.

In periodic MOF structures, single metal ions or metal ion clusters act as vertices and are linked typically by rigid polydentate ligands, such as carboxylates.²⁵ A vertex characterized by a specific ligand topology around metal ion centers is often referred to as a secondary building unit (SBU)²⁶ and is useful for understanding and classifying MOF structures. Experimentalists have commonly opted for transition metal ions as the cationic counterparts in MOFs due to their preferences for a wide range of strong coordination geometries, thereby enabling modification and fine-tuning of MOF structures and properties.²⁷

The relative flexibility of a Zn^{2+} ion to adopt various coordination geometries in the presence of different ligands has given rise to a multitude of MOFs that can be broadly classified into two categories. The MOFs in the first category consist of Zn^{2+} ions (either as isolated ions or as clusters) and aromatic carboxylate ligands,²⁸ while those in the second category consist of Zn^{2+} ions and imidazolate ligands and are known as zeolitic imidazolate frameworks (ZIFs).²⁹ The Zn^{2+} ions in ZIFs, with zeolite-like topologies, have tetrahedral coordination geometries, whereas the Zn^{2+} ions in carboxylate ligand based MOFs adopt a variety of coordination geometries (including tetrahedral). MOF-2 (with the structural formula, $Zn(BDC)(DMF)(H_2O)$) was one of the first carboxylate ligand based MOF structures reported in the literature.³⁰ MOF-2, a two-dimensional layered network structure (see Figure 1a), can be seen as an archetype for a subclass of MOFs composed of SBUs that are binuclear metal ion clusters in a paddle-wheel cluster (PWC) arrangement.³¹ Each PWC comprises two Zn^{2+} ions bridged by four carboxylate units, each from a BDC ligand in a monodentate fashion (see Figure 1b). Some experimental studies reveal that formation of a MOF-2-like structure can apparently occur in multiple types of polar solvents (*e.g.*, DMF³² and DMSO³³) at different temperature conditions. While one particular experiment³⁴ revealed that a MOF-3-like structure (see Figure 1c), consisting of SBUs with Zn -ion triplets as the vertices³⁵ (see Figure 1d), was formed as a metastable structure prior to production of the target MOF-2 structure, metastable structures for other MOFs³⁶ have been reported, as well. Moreover, PWC-like structural motifs are found not only in infinite coordination polymers (1-D chains, 2-D nets, and 3-D framework structures) but also in discrete coordination complexes.³¹ Accordingly, a system consisting primarily of Zn^{2+} ions and 1,4-benzenedicarboxylate (BDC) ligands, with a MOF-2-like target structure, can be considered a suitable prototypical candidate for examining self-assembly processes to help reveal general aspects of the mechanism of formation.

The present study utilizes atomistic models with an explicit solvent in molecular dynamics (MD) simulations to explore the

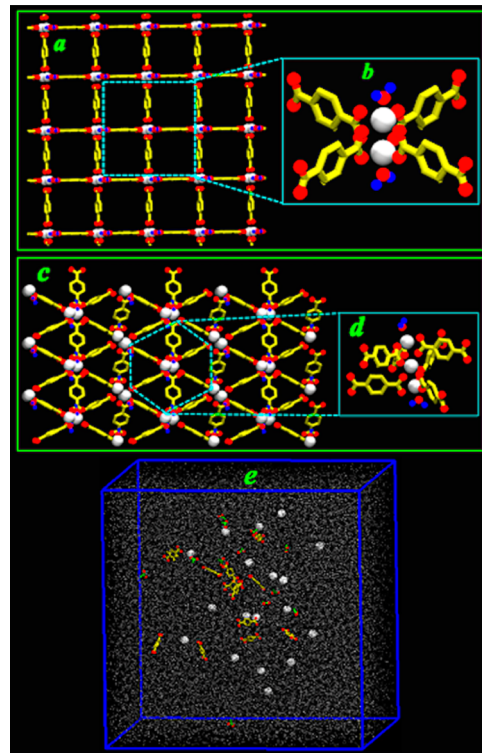


Figure 1. (a) Periodic MOF-2 structure;²⁵ (b) paddle-wheel cluster; (c) periodic MOF-3 structure;³⁵ (d) trimeric Zn -ion cluster; (e) initial configuration of a S_{18} system in a typical simulation box, where solvents are shown as points to allow the Zn ions and ligands to be seen. The model Zn ions, BDC ligands, and acetate ions (monodentate ligands) are white, yellow, and green, respectively.

mechanisms of self-assembly of an archetypal Zn -carboxylate MOF, where the focus is on the previously unreported early stages of the underlying ordering processes. To this end, simple yet efficient models representing metal ions, ligands, and solvent molecules were used in MD simulations to achieve successful assembly of multiple MOF-2-like square arrangements. Notably, the self-assembly processes in both explicit and continuum solvent simulations were examined. The results for these Zn -carboxylate MOF systems suggest a plausible mechanism that features a structural ordering hierarchy, characterized by multiple intermediate structures, where such behavior is also observed for other nanostructured materials such as peptide nanotubes and nanovesicles.³⁷

RESULTS AND DISCUSSION

Selected Models. A typical solution from which a MOF might assemble, featuring components such as transition metal ions, bulky organic carboxylate ligands, counterions, and mixed solvents, represents a relatively complex system to model. The self-assembly of MOFs usually spans a wide range of time scales, from several minutes to several days, depending on the particular synthetic technique being employed. Such experimental time scales are clearly inaccessible to molecular simulations. To achieve a fundamental understanding of the processes associated with formation of MOF-like structures, the utilization of relatively simple models in MD simulations is necessary to facilitate investigation and interpretation of the results. The physical models employed in this study consider the principal components (*i.e.*, the BDC ligand, the Zn -ion, and the solvent) common to a variety of MOF structures, including

MOF-2, and incorporate their key attributes to reasonably reproduce the stability and final structure of MOF-2. In the current study, a mixture of BDC and acetate ligands was used primarily for two reasons: (1) to allow formation of discrete MOF-2-like square arrangements of PWCs or other finite structures in the system where the acetate ion serves as a capping role as a monotopic ligand; (2) to allow a mixture of mono- and ditopic carboxylate ligands to more appropriately represent the early stages of self-assembly for experimental MOF-2-like systems where slow deprotonation of BDC ligands is a crucial step. Similar simple but effective modeling approaches have been adopted for exploring the self-assembly processes in other systems.^{22–24,38} Further details of the models employed can be found in the [Supporting Information](#).

Three different solvent models were considered, a dipolar solvent, a dimethylformamide (DMF) solvent, and a continuum solvent ($\epsilon = 2, 2.5$, and 3). Although exploring the molecular-level self-assembly processes in explicit solvent simulations was the principal focus of the current study, the continuum solvent model was used to allow comparisons to be made to earlier simulation studies^{22–24} and to assess the reliability of continuum solvent models. A value of $\epsilon = 2$ for the continuum solvent, which has been used in previous MOF simulations,^{22–24} was found to provide behavior most similar to that of explicit solvent systems. Hence, although this dielectric constant does not correspond to any realistic solvent, it will be used in most of the comparisons below. DMF is typically employed as a solvent in experiments of Zn-carboxylate MOFs. Therefore, DMF solvent simulations were performed both to explore the structural evolution in a more realistic solvent medium and to provide a basis of comparison for the effectiveness of the dipolar solvent model that was extensively studied.

Two system sizes were examined systematically: the smaller system containing eight Zn ions together with four BDC and eight acetate ligands, and the larger system containing 18 Zn ions with 12 BDC and 12 acetate ligands (see [Figure 1e](#)). The systems containing eight Zn ions in dipolar, DMF, and continuum solvents are referred to as S_8 , $S_{\text{DMF}8}$, and $S_{\text{LD}8}$, respectively. Similarly, the systems containing 18 Zn ions in dipolar, DMF, and continuum solvents are referred to as S_{18} , $S_{\text{DMF}18}$, and $S_{\text{LD}18}$, respectively. To probe larger length scale self-assembling events, simulations both of systems containing 72 Zn ions together with 56 BDC ligands and 32 acetate ions in dipolar solvent and continuum solvent (labeled as S_{72} and $S_{\text{LD}72}$, respectively) and of a system containing 200 Zn ions with 180 BDC ligands and 40 acetate ions in dipolar solvent (labeled as S_{200}) were performed. While multiple trajectories were generated for the smaller S_8 and S_{18} systems, only a limited number of trajectories could be generated for the larger S_{72} and S_{200} systems owing to their high computational cost (see the [Supporting Information](#)). The four system sizes chosen for this study represent supersaturated solutions with Zn-ion concentrations corresponding roughly to those typically used in the experiments (see the [Supporting Information](#)). The specifics for the various systems investigated, including the numbers of the different species in each of these systems, can be found in the [Supporting Information](#).

Identification of Topological Elements. The behavior of systems with each of the three solvents was examined in detail, and the similarities and differences of their structural evolution were explored. To facilitate these discussions, it will be advantageous to focus first on characterizing behavior in the

S_8 , S_{18} , S_{72} , and S_{200} systems (*i.e.*, systems with a dipolar solvent). It will also be useful in the structural discussions below to identify “topological elements”, where this term refers to a unit cell or similar assemblies featuring SBUs linked together by ligands into various geometric shapes such as triangles, squares, pentagons, etc. [Figure 2](#) provides examples of

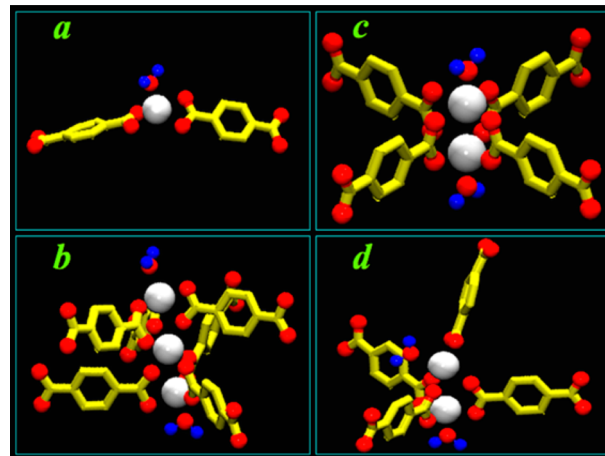


Figure 2. Common SBUs found in experiments and the current simulations: (a) represents the vertex of a 1-D-like coordination polymer;³⁴ (b,c) correspond to SBUs of MOF-3-like and MOF-2 structures, respectively;^{30,34,35} (d) represents a three-blade paddle-wheel cluster (PWC-3), where a pair of Zn ions are bridged by three BDC ligands, and a fourth BDC ligand is seen coordinated to one of the Zn ions. The water molecules shown (in red and blue CPK presentation) are typically found in experimental structures and were not incorporated into the current simulations. Ions and ligands appear as in [Figure 1](#).

different types of Zn-ion SBUs observed in experiments and in the current simulations. The triangle-shaped arrangement of Zn ions and BDC ligands in a MOF-3-like structure and square-shaped arrangement of PWCs in a MOF-2-like structure can be identified as two different examples of topological elements. In the simulations reported here, multiple types of topological elements are observed during the self-assembly process, where these topological elements existed either as part of some larger structural aggregate or as discrete structural units.

General Aspects of Structural Evolution. The simulations reported here reveal three critical aspects of MOF self-assembly: (1) various ordering processes occur in multiple stages; (2) multiple types of Zn-ion clusters are generated; (3) combinations of the different types of Zn-ion clusters lead to formation of multiple types of topological elements, thereby producing complex structures during the early stages of self-assembly. For the S_8 (*i.e.*, dipolar solvent) system, seven out of the 30 simulations successfully produced a MOF-2-like square topological element structure within a 50–250 ns time scale. This range of times can be attributed to the stochastic nature of the self-assembly process. [Figure 3](#) shows evolution of the potential energy and snapshots from a typical trajectory for a S_8 system that successfully self-assembled into a discrete unit cell in ~200 ns. Snapshots from two other trajectories for this system are provided in the [Supporting Information](#).

Visualization of the trajectories revealed octahedral Zn ions coordinated by dipolar solvent molecules at the beginning of the simulations (see [Figure S5](#)); an octahedral coordination geometry of Zn ions is typical in polar solvents such as water,³⁹

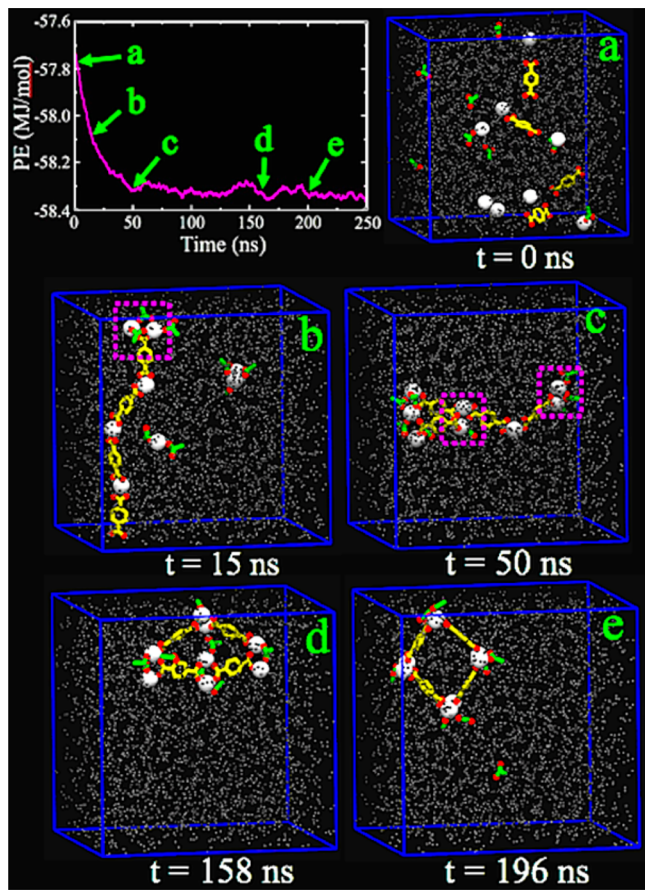


Figure 3. Potential energy of the system (top left) and snapshots of the system at various stages (a–e) of the self-assembly process of a MOF-2-like square topological element structure observed in a typical trajectory of a S_8 system. Ions and ligands appear as in Figure 1. Solvent molecules are shown as points for visual clarity, and figures are shaded by depth. In the panels (b) and (c), the rectangular boxes in magenta show PWC-3 motifs formed during the structural evolution. A near-perfect MOF-2-like square topological element structure was achieved in this trajectory through a quenching in the solvent polarity. The plot of potential energy is labeled with the corresponding molecular configurations shown in panels (a–e).

methanol,⁴⁰ ethanol,⁴⁰ and DMF.⁴⁰ Gradually, the carboxylate ligands replace the solvent molecules in the coordination shells of the Zn ions in several possible structural combinations (see Figure S5) that are reminiscent of various Zn-carboxylate coordination modes reported in the literature.⁴¹ The initial aggregation of Zn ions and carboxylate ligands results primarily in formation of 1-D chain-like fragments, typically within the first ~10 ns of the simulations (see Figure 3b), that consist primarily of single Zn ions and some Zn-ion pairs. The Zn-ion pairs formed at this stage are generally bridged by two carboxylate ligands. More ordered Zn-ion pairs (*e.g.*, bridged by three or more carboxylate groups) are rare events during the first stage of self-assembly in these systems.

Concurrent with the configurational changes of the system, the potential energy of the system decreases (see Figure 3). Within the first ~50 ns of the S_8 system simulations, the 1-D chain-like fragments assemble and rearrange to form different types of Zn-ion clusters (see Figure 3c), such as Zn-ion pairs, triplets, and quadruplets, as vertices of larger assemblies. These different types of vertices or SBUs are formed as constituent

components of the growing assemblies, and do not typically exist as independent units in the system. Later, a slow reorganization stage was observed in the structural evolution during which various topological elements composed of different types of linked SBUs, including a discrete MOF-2-like square topological element, were produced. The relatively small size of S_8 systems typically allowed only one particular type of topological element to be present at any time during this reorganization stage, although interconversions between different types of topological elements were observed, such as conversion of triangular topological elements (discussed below) to MOF-2-like square topological elements or *vice versa*.

Figures 4 and 5 show snapshots from a typical trajectory of the S_{18} system and from the trajectory of the S_{200} system, respectively. Snapshots from another trajectory for the S_{18} system is provided in the Supporting Information (Figures S4), and Figure S6 shows selected snapshots from the trajectory of the S_{72} system. Visualization of the trajectories along with other qualitative analyses demonstrate that the basic mechanistic features of the self-assembly process in the S_{18} , S_{72} , and S_{200} systems are generally similar to those in the S_8 systems and are characterized by initial production of 1-D chain-like fragments within roughly the first ~10 ns (see Figures 4a and 5a), with the emergence of various 2- and 3-D arrangements between ~20 and 100 ns followed by a slow reorganization stage. The larger sizes of the S_{18} , S_{72} , and S_{200} systems enabled formation of various types of topological elements in more complex structural arrangements (see Figures 4c–f and 5c) during the reorganization stage; for example, triangular topological elements are found to share their edges with other triangular or square-shaped topological elements. During the third reorganization stage of the S_{72} and S_{200} systems, the Zn ions and carboxylate ligands were observed to form a single conglomerate (see Figure 5c), composed of various component structures (see insets in Figure 5c) that are, in turn, composed of combinations of topological elements. The component structures identifiable within the conglomerate shown in Figure 5c are reminiscent of the structures assembled in smaller S_{18} systems (see Figure 4). Similar observations can be made for the S_{72} (see Figure S6) and S_{1872} systems and provide confirmation of the common mechanistic features of the self-assembly process across the range of system sizes. It is generally observed that the overall level of complexity of the amorphous entity produced during the reorganization stage increases, as expected, with increasing numbers of Zn ions and carboxylate ligands in the system as more topological elements become linked together. An additional set of explicit dipolar solvent simulations was performed for S_{18} systems to investigate the possible effects of increased Zn-ion concentration on the self-assembly processes. The effect of this change in Zn-ion concentration was observed to somewhat influence the formation rates of various cluster sizes without otherwise impacting the underlying mechanisms (see the Supporting Information).

Competing Kinetic Structures. Figure 6 shows several of the commonly observed topological elements among which three-membered rings (see Figure 6a–d) were most abundant across the different system sizes, as seen at the end of ~70% of the trajectories for the S_8 system. These three-membered ring structures contained vertices consisting of either single Zn ions, Zn-ion pairs, or Zn-ion triplets. The two Zn ions in a pair are usually bridged by either two or three carboxylates, whereas the three Zn ions in a triplet are typically bridged by five or six

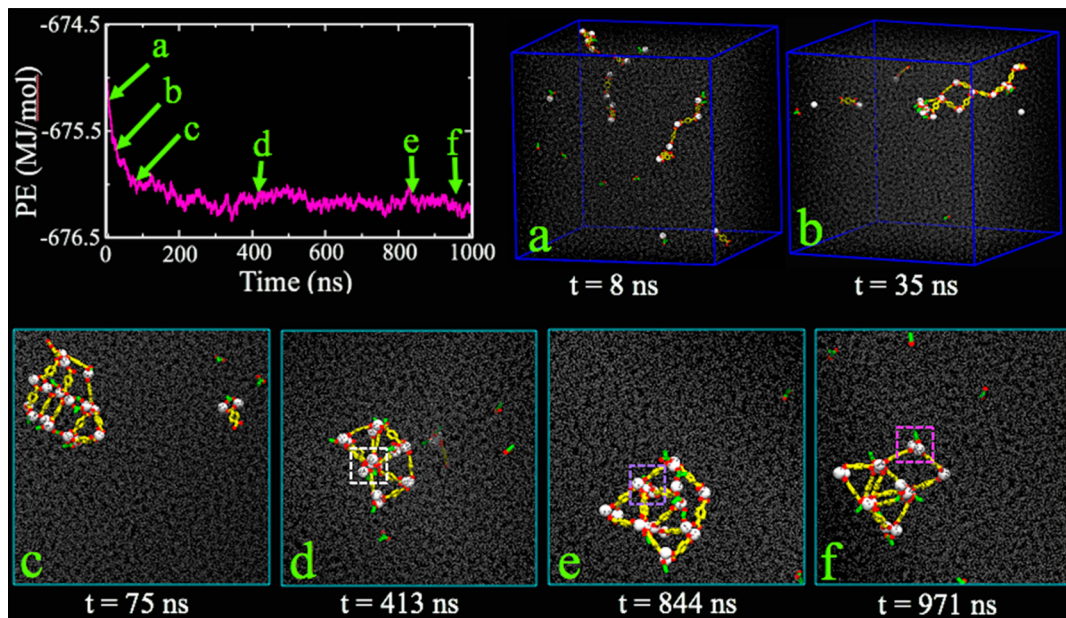


Figure 4. Potential energy of the system (top left) and snapshots of the system at various stages (a–f) of the self-assembly process observed in a typical trajectory of a S_{18} system. The plot of potential energy of the system is labeled with the corresponding molecular configurations shown in panels (a–f). Ions and ligands appear as in Figure 1. (c–f) Enlarged images of the structures for visual clarity. The rectangular boxes in white (d), purple (e), and magenta (f) show examples of four Zn ions in a cluster, a Zn-ion triplet, and a Zn-ion pair in the PWC-3 structure, respectively.

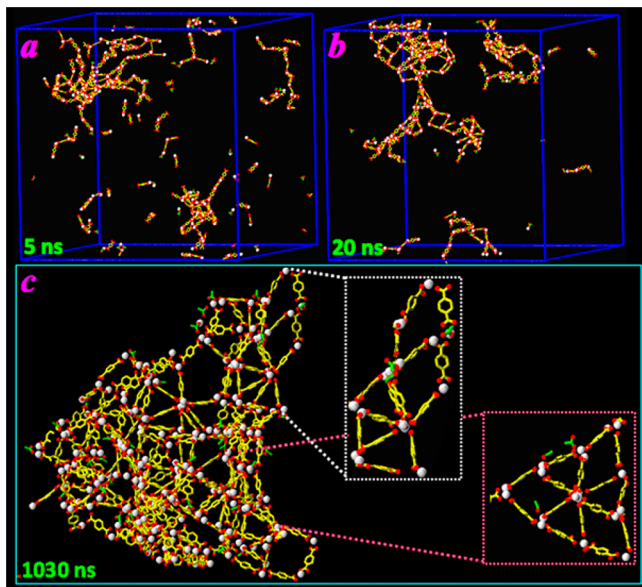


Figure 5. Snapshots of the system at various stages (a–c) of the self-assembly process observed in the trajectory of the S_{200} system. Ions and ligands appear as in Figure 1. Solvent molecules are omitted for visual clarity. In panel (c), the insets show enlarged images of two examples of component structures observed within the amorphous conglomerate. Each of these component structures consists of approximately 18 Zn ions.

carboxylates. Based on the number of Zn ions at its vertices, either triangular (see Figure 6c) or triangle with an arm-like topological elements (see Figure 6a,b) were observed. Triangular topological elements as well as other topological elements such as squares (see Figure 6e) and layered structures (see Figure 6f) found in the simulations can be interpreted as competing kinetic structures. Notably triangular structures are

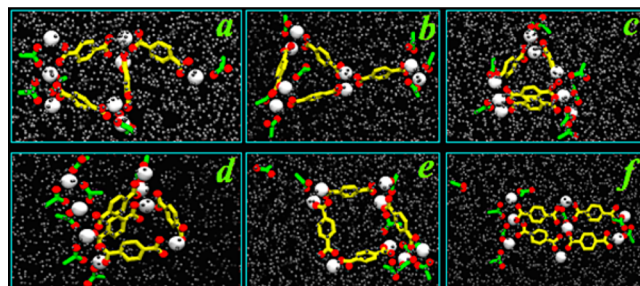


Figure 6. Common topological elements (a–f) found in the simulations of S_8 and S_{18} systems (in addition to a MOF-2-like square arrangement of PWCs). Ions and ligands appear as in Figure 1. (a–d) Examples of triangular topological elements, (e) square topological element, and (f) layered topological element.

known to constitute the unit cells in several MOF structures (e.g., MOF-3³⁵ and analogous MOF structures).^{32,34,42} Similarly, layered arrangements of metal ions and ditopic carboxylate ligands are observed in several MOFs or coordination polymers (e.g., Na ion, K ion, Mg ion, Zn ion, etc.^{34,43,44}).

Potential Energy of the System. Analysis of the evolution of the potential energy (PE) can also help reveal aspects of the underlying relaxation stages of these systems. Figure 7 shows the time evolution of PE distributions and of the average PE with respect to the 30 and 10 trajectories for S_8 and S_{18} systems, respectively. As can be seen from Figure 7b,d, the average PEs, representative of an ensemble of structures, exhibit apparent exponential decay for both S_8 and S_{18} systems. Therefore, multiexponential fitting of the average S_8 and S_{18} PE curves, namely, $y = a_0 + a_1 e^{-t/\tau_1} + a_2 e^{-t/\tau_2} + a_3 e^{-t/\tau_3}$, was performed, and Table 1 lists the relaxation times obtained. The multiexponential fits revealed two and three modes of relaxation for S_8 and S_{18} systems, respectively. Notably, a

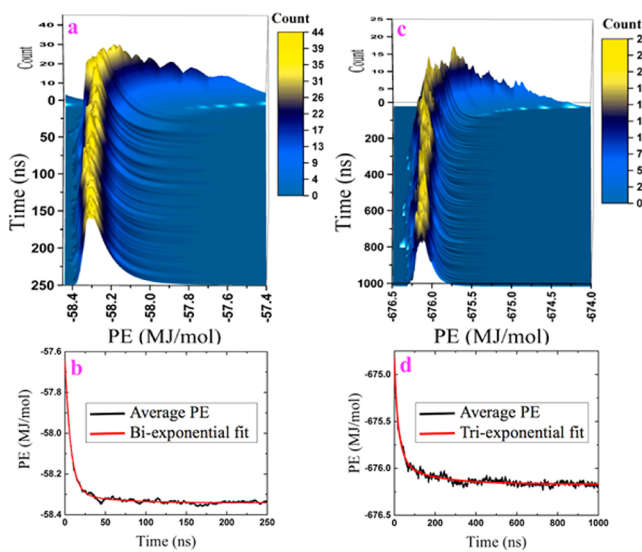


Figure 7. (a,c) Time evolution of PE distributions for S_8 and S_{18} systems, respectively. (b,d) Time evolution of the average PEs along with their exponential fits for S_8 and S_{18} systems, respectively.

Table 1. Coefficients of Exponential Fits of the Average PEs for S_8 and S_{18} Systems

coefficient	S_8	S_{18}
τ_1 (ns)	7	8
τ_2 (ns)	49	25
τ_3 (ns)		180

triaxponential fit for the S_8 systems resulted in no clear improvement in the fit and two fast relaxation times of essentially the same value. The apparent absence of a third relaxation mode (characterized by the relaxation time τ_3) for the S_8 systems can presumably be attributed to its relatively small size and lack of structures composed of multiple topological elements. It is interesting to note that the fast relaxation times for S_{18} and S_8 systems are in good agreement, thereby indicating the occurrence of similar events in the initial stage of self-assembly; when compared with visualizations of the simulation trajectories, this fast relaxation mode appears to correspond to the production of 1-D chain-like fragments at the first stage of structural evolution. Similar multiexponential fits of the PE curves resulting from the single trajectories for the S_{72} and S_{200} systems again revealed at least three relaxation modes, where the fast relaxation times were found to be in good agreement with that of S_{18} and S_8 systems. The multiexponential behavior in the PE signals the existence of a series of relaxation processes in these model systems, where such behavior is typical for systems with complex free energy landscapes such as proteins.⁴⁵

Cluster Size Distributions. The sizes of the Zn-ion clusters can be used to investigate and further characterize the general ordering processes in both S_8 and S_{18} systems. Although an experimental MOF-2-like structure would consist exclusively of Zn-ion pairs and PWC (or PWC-4) SBUs (*i.e.*, a PWC with four bridging carboxylates), several other types of SBUs were also found to form during these simulations. To help characterize the Zn-ion clusters that appear as components of topological elements, cluster size distributions and their time evolutions were examined. In this analysis, Zn ions were considered part of the same cluster if the Zn–Zn distance was

$\leq 5 \text{ \AA}$, where this cutoff value was determined from the Zn–Zn radial distribution function for these systems. In this way, Zn clusters of size 2, size 3, size 4, and size 5 were identified, and the numbers of clusters ($N_{\text{cluster}}^{\alpha}$) of size α were calculated.

Figure 8 shows the time evolution of normalized fractions of clusters ($N_{\text{cluster}}^{\alpha}/N_{\text{max}}^{\alpha}$) for different cluster sizes (*i.e.*, single Zn

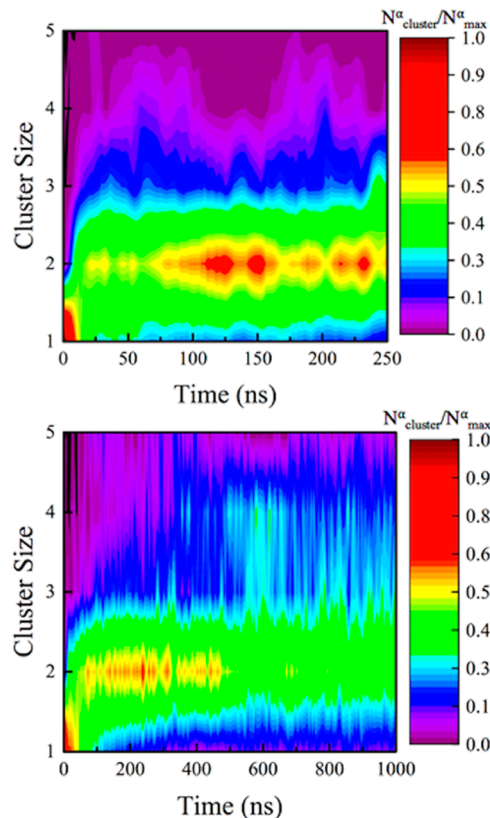


Figure 8. Evolution of the normalized fraction (by maximum number possible) of Zn-ion clusters ($N_{\text{cluster}}^{\alpha}/N_{\text{max}}^{\alpha}$) for different cluster sizes in both S_8 (top panel) and S_{18} (bottom panel) systems.

ions, size 2, size 3, size 4, and size 5 clusters), where N_{max}^{α} represents the maximum number of clusters possible for the particular cluster size, α . It should be noted that values obtained for these normalized fractions would also equal the ratio of the number of Zn ions found in clusters of size α to total number of Zn ions in the system. These fractions were again averaged over the 30 trajectories for S_8 and the 10 trajectories for S_{18} systems. The overall growth trends appear similar for both the S_8 and S_{18} systems. A prominent feature in both the systems is the predominance of size 2 clusters (~50%) relative to other sizes. This is suggestive of a greater propensity for Zn ions to form pairs. Initially, the fraction of single Zn ions in the systems decreases rapidly with time, and clusters (size 2, size 3, size 4, and size-5) begin to appear (see **Figure 8**), although the initial growth rate of size 2 clusters is much higher than that of larger cluster sizes. The curve for the size 2 clusters reaches a slower relaxation stage at ~25 ns for the S_8 systems and ~100 ns for the S_{18} system. The curves of other cluster sizes also exhibit slow relaxation stages, indicating the onset of very slow reorganization dynamics in these systems that resembles a pseudo-steady state (*i.e.*, the overall relaxation time appears long in comparison with the time scale of the ongoing rearrangements of the topological elements). A multiexponen-

tial fitting (similar to the average PE) was also applied to the apparent exponential decay in the evolution of the population of single Zn ions for both S_8 and S_{18} systems. These fits revealed multiple relaxations, where the fastest relaxation modes (with times of 9 and 6 ns for the S_{18} and S_8 systems, respectively) were consistent with those obtained from average PEs (see Table 1).

While the cluster size distributions of Zn-ion clusters revealed important insights, it is useful to explore the relationship between cluster size and ligand coordination. Figure 9a,b shows time evolution of normalized fractions of Zn-

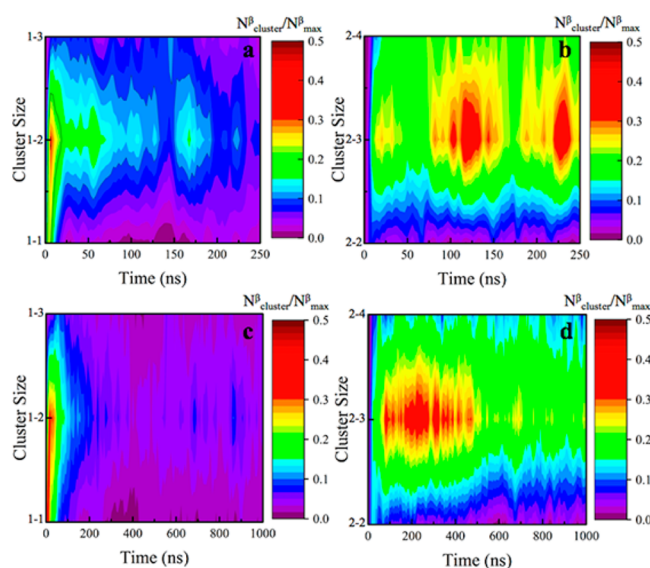


Figure 9. Evolution of the normalized fraction (by maximum number possible) of Zn-ligand clusters ($N_{\text{cluster}}^{\beta}/N_{\text{max}}^{\beta}$) for different cluster sizes. Single Zn ions coordinated to one, two, and three ligands are denoted as 1–1, 1–2, and 1–3 clusters, respectively. Zn-ion pairs coordinated to two, three, and four ligands are labeled as 2–2, 2–3, and 2–4 clusters, respectively. Panels (a,c) show 1–1, 1–2, and 1–3 clusters for S_8 and S_{18} systems, respectively. Panels (b,d) show 2–2, 2–3, and 2–4 clusters for S_8 and S_{18} systems, respectively.

ligand clusters ($N_{\text{cluster}}^{\beta}/N_{\text{max}}^{\beta}$) for different cluster sizes (β) for the S_8 system, and Figure 9c,d provides the same for the S_{18} system. A particular Zn-ligand cluster size, β , depends on the number of Zn ions and the number of surrounding carboxylates, where a cutoff distance of 4 Å was used for the Zn ion and oxygen atom separation. This value was determined from the Zn–O radial distribution function for these systems. In this way, 1–1, 1–2, and 1–3 clusters (see Figure 9a,c) that correspond to single Zn ions coordinated to one, two, and three ligands, respectively, were identified. Similarly, 2–2, 2–3, and 2–4 clusters (Figure 9b,d) refer to a pair of Zn ions coordinated to two, three, and four carboxylate groups, respectively. Consistent with the time evolution behavior of Zn-ion clusters, the number of 1–1, 1–2, and 1–3 clusters decreased with time after a very rapid initial increase for both the systems. The time evolutions of 2–2 clusters, representing less ordered structures, displayed an initial increase followed by a gradual decrease in number, where such behavior is consistent with visual analyses. The 1–1 or 1–2 clusters formed during the earlier stages coordinate to additional carboxylate groups or other Zn-ligand clusters and then rearrange to produce more ordered structures, such as the 2–3 and 2–4 clusters. It is

evident from the Figure 9 that 2–3 and 2–4 clusters constitute the major type of Zn-ligand clusters in both S_8 and S_{18} systems, with 2–3 clusters having a slightly higher probability of forming. The topology of a 2–4 cluster, as revealed from visualization of simulation trajectories in both S_8 and S_{18} systems, is typically not that of a PWC-4 but rather tends to resemble a PWC-3 motif (*i.e.*, a PWC bridged by three carboxylates) with an extra nonbridging carboxylate group coordinated to one of the Zn ions (see Figure 2d). Furthermore, 2–3 clusters were mostly PWC-3 SBUs that are components of triangular, square, or pentagonal topological elements. Notably, PWC-3 motifs are known to form in several coordination polymers and MOFs composed from a wide variety of metal ions, including Zn ions³¹ and carboxylate ligands.

Figure 10 shows averaged values of $N_{\text{cluster}}^{\alpha}/N_{\text{max}}^{\alpha}$ for different cluster sizes for the S_8 , S_{18} , S_{72} , and S_{200} systems. These

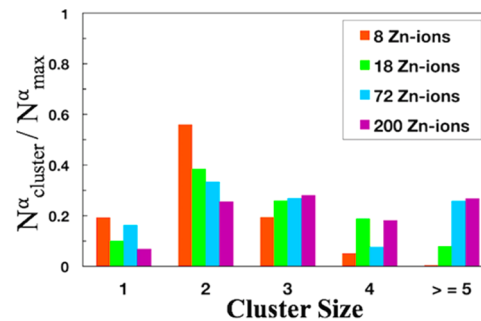


Figure 10. Average normalized fractions (by maximum number possible) of Zn-ion clusters ($N_{\text{cluster}}^{\alpha}/N_{\text{max}}^{\alpha}$) for different cluster sizes in S_8 (orange bars), S_{18} (green bars), S_{72} (cyan bars), and S_{200} (purple bars) systems. The averaging was performed over last 100 ns in 30 trajectories for S_8 , 10 trajectories for S_{18} , and single trajectories each for the S_{72} and S_{200} systems, resulting in larger uncertainties in the results for the latter systems.

fractions were averaged over the last 100 ns of the corresponding trajectories for each of these system sizes; although these values are averaged over 30 and 10 trajectories for S_8 and S_{18} systems, respectively, averages correspond to the single trajectories for both S_{72} and S_{200} systems. Figure 10 together with other cluster size analyses reveals that the basic structural characteristics of the larger systems are in accord with those observed in the smaller S_8 and S_{18} systems. For example, size 2 Zn-ion clusters (see Figure 10) and 2–3 Zn-ligand clusters (see Figure S7) remain generally the predominant type of clusters in these systems, although S_{72} and S_{200} systems exhibit a slightly higher propensity to form larger cluster sizes (*e.g.*, size 4 and size 5 clusters). In general, it can be anticipated that for smaller system sizes the limited number of Zn ions available will impact the probability of observing larger Zn clusters; for example, in a S_8 system, the probability of a size 5 cluster is very low. However, given the single trajectory statistics associated with the S_{72} and S_{200} system results, the apparent differences in cluster size distribution behavior for these systems (relative to S_{18} system) cannot be distinguished from errors arising from insufficient sampling.

An additional factor influencing the Zn-ion cluster size distributions in the four S_n systems (illustrated in Figure 10), is the ratio of ditopic (BDC) to monotopic (acetate ion) ligands in the system. The numbers of monotopic and ditopic carboxylate ligands in the different simulation systems were

initially chosen to facilitate formation of finite structures composed of specific numbers of discrete structures with MOF-2-like square arrangements of PWCs in an ideal situation. With an increasing number of Zn ions in the four S_n systems, this ligand ratio increased significantly; specifically, the ratios of ditopic BDC to monotopic acetate ligands are 1:2, 1:1, 1.75:1, and 4.5:1 in S_8 , S_{18} , S_{72} , and S_{200} systems, respectively. This increasing ratio of ditopic BDC to monotopic acetate ligands in these systems can also be regarded as a preliminary investigation of the possible effects of a slow deprotonation process (*i.e.*, the slow conversion of carboxylic acids to carboxylate ligands, common to most experiments) on the structural behavior of the system during the early stages of the self-assembly process. To explore this behavior more directly, that is, the effect of increasing numbers of ditopic relative to monotopic ligands on the structural organization process, additional simulations were performed (see Table S3 in the **Supporting Information**). In particular, three different ratios of BDC to acetate ligands, 1:2, 1:1, and 1.75:1, were examined for S_{18} , S_{LD18} , and S_{LD72} systems in explicit and continuum solvent simulations, where multiple simulation trajectories were generated for each. Also, explicit solvent systems incorporating 18 Zn ions and 36 monotopic carboxylate ligands (both monotopic acetates and monotopic BDCs) were carried out to investigate the influence of monotopic carboxylate ligands on structural behavior in the absence of ditopic carboxylate ligands.

Cluster size distribution analyses (see Figure S8 in the **Supporting Information**) of S_{LD72} systems revealed that when the ratio between BDC and acetate ligands is 1:2, the number of single Zn ions remains relatively high (and here roughly equal to the proportion of size 2 clusters). As the number of BDC ligands increases relative to the acetates, the number of size 2 Zn-ion clusters increases in the system. When the ratio between BDC and acetate ligands is 1:1 or 1.75:1, size 2 Zn-ion clusters and 2–3 Zn-carboxylate clusters become the predominant type of vertices in the system. Additionally, the proportion of 2–4 Zn-ligand clusters relative to 2–3 clusters also increases with increasing numbers of BDC ligands in the system. Similar structural evolution features were also observed for the S_{18} and S_{LD18} systems; that is, the number of size 2 Zn-ion clusters tends to increase when the ratio of BDC to acetate ligands increases. These characteristic trends were observed to be apparently independent of the type of monotopic carboxylate ligand employed in the systems; the systems incorporating monotopic BDC ligands exhibited structural behavior very similar to those incorporating monotopic acetate ligands. A strong inclination toward formation of size 2 Zn-ion clusters was also exhibited by systems incorporating monotopic carboxylate ligands exclusively, where these systems strongly favored formation of smaller cluster sizes.

Solvent Dependence. To investigate how, in general, different solvent models may affect MOF self-assembly, dipolar, DMF, and continuum solvents were each examined in sets of simulations. In accord with experimental observations of formation of MOF-2-like structures from Zn-ion and BDC-containing systems in a variety of solvent environments, successful formation of MOF-2-like square arrangements of PWCs was observed in simulations with each of these three different solvents. In the continuum solvent simulations, the electrostatic interaction strength between Zn ions and carboxylate ligands is scaled by the dielectric constant of the solvent medium. The selected value ($\epsilon = 2$) helps to promote a relatively fast structural reorganization and, therefore, a higher

rate of sampling of the underlying free energy landscape, as compared to the explicit solvent simulations. Yet, continuum solvent simulations with $\epsilon > 2$ exhibit formation of structures somewhat different from those observed with $\epsilon = 2$ (*e.g.*, increased populations of single Zn ions for $\epsilon = 2.5$). Consistent with these continuum solvent simulations, results from simulations employing explicit dipolar solvents indicate that more polar solvents tend to destabilize various ordered structures (*e.g.*, PWCs), whereas less polar solvent systems (compared to those using sol-0.55) exhibit considerably slower relaxation dynamics.

Figure 11a–c shows the time evolution of the normalized fraction of clusters ($N_{\text{cluster}}^{\alpha}/N_{\text{max}}^{\alpha}$) for different cluster sizes for

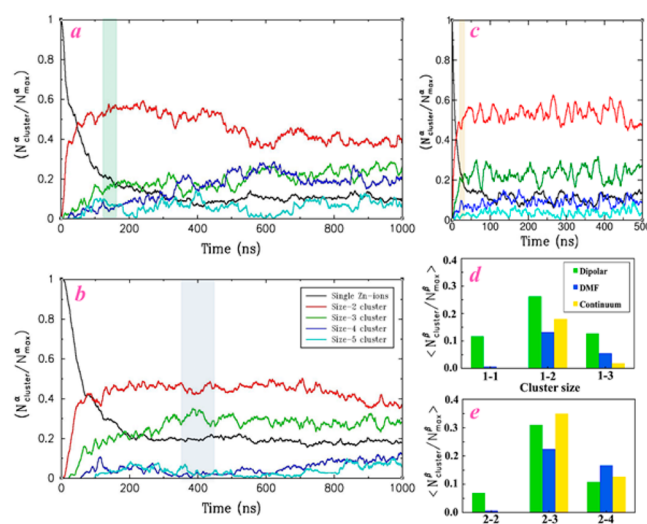


Figure 11. Solvent dependence of the normalized fraction (by maximum number possible) of Zn-ion clusters ($N_{\text{cluster}}^{\alpha}/N_{\text{max}}^{\alpha}$) for different cluster sizes in systems containing 18 Zn ions. Evolution of $N_{\text{cluster}}^{\alpha}/N_{\text{max}}^{\alpha}$ in S_{18} , S_{DMF18} and S_{LD18} systems are shown in (a–c), respectively. In panels (a–c), the black, red, green, blue, and cyan curves represent single Zn ions, size 2, size 3, size 4, and size 5 clusters, respectively. (d) Comparison of the average normalized fraction of 1–1, 1–2, and 1–3 Zn-ligand clusters for S_{18} (green bar), S_{DMF18} (blue bar), and S_{LD18} (orange bar) systems. (e) Comparison of the average normalized fraction of 2–2, 2–3, and 2–4 Zn-ligand clusters for S_{18} (green bar), S_{DMF18} (blue bar), and S_{LD18} (orange bar) systems. The averaging in panels (d,e) was performed between 25 and 30 ns (shaded area in (c)), 125–160 ns (shaded area in (a)), and 350–450 ns (shaded area in (b)) for S_{LD18} , S_{18} , and S_{DMF18} systems, respectively. The time windows for averaging, in different solvent systems, were selected for when the fractional population of single Zn ions in these systems had decayed to 0.2.

the S_{18} , S_{DMF18} , and S_{LD18} systems, respectively (see Figure S9 for the analogous comparison for different cluster sizes in S_8 , S_{DMF8} , and S_{LD8} systems). When the evolution is compared for the three solvent systems, a temporal shift in the occurrences of similar events is typically observed; for example, the rates of various ordering processes in systems with a discrete solvent are decreased by a factor of ~5–10 compared to the systems with a continuum solvent.

In order to explore the specific differences of clustering events in these systems, relative time windows were used to calculate and compare the average normalized fraction of Zn-ligand clusters, $\langle N_{\text{cluster}}^{\beta}/N_{\text{max}}^{\beta} \rangle$, for different cluster sizes, β . Specifically, the averaging was performed over all trajectories

within time windows of 25–30 s, 125–160, and 350–450 ns for the S_{LD18} , S_{18} , and S_{DMF18} systems, respectively; these times were chosen because they each correspond to when the fractional population of single Zn ions had decayed to ~0.2. Figure 11d,e shows comparisons of these average values for various Zn-ligand cluster sizes in these systems (see Figures S10 and S11 for average normalized fractions of Zn-ligand clusters for different cluster sizes in S_8 , S_{DMF8} , and S_{LD8} systems). A comparison of these distributions for the three solvent models reveals that they have general similarities (e.g., the 1–2 and 2–3 clusters being preferred). However, differences are apparent in the specific fractions of various Zn-ligand cluster sizes, suggestive of differences in relative stabilities of the various arrangements (*i.e.*, Zn-ion clusters and topological elements) in the three solvents, details of which will be explored in future work.

Visualization of simulation trajectories for the systems with DMF and continuum solvents revealed mechanistic features of the self-assembly process similar to those observed with the dipolar solvent. All of these systems demonstrate formation of 1-D chain-like fragments, the assembly of topological elements, and then the interconversion of the topological elements during a slow reorganization stage. It can be inferred from these observations that the general features of structural evolution of Zn-ion and carboxylate-ligand systems in various solvent media (e.g., importance of size 2 clusters) are reasonably robust, although the details of the self-assembly (e.g., the fraction of different cluster types) can be sensitive to solvent choices. Analysis of the topological elements that appear at the end of trajectories reveals that triangular and square topological elements (as in Figure 6e) are the predominant types. However, better statistics (*i.e.*, a significantly larger number of trajectories particularly for larger systems) would be required to characterize such differences quantitatively.

It should be noted that ~80 and ~10% of the trajectories in the S_{LD8} and S_{DMF8} systems, respectively, produced a MOF-2-like square topological element at the end of their respective simulations in comparison with the ~20% observed in the S_8 system. The persistence time of a MOF-2-like square topological element also depends on the choice of solvent. For example, it was observed in the S_{LD8} system that a discrete MOF-2-like square topological element is not a long-lived structure once formed but rather converts readily into other types of topological elements. Considering the longer time scales associated with reorganizational events in the S_{DMF8} system (relative to those with the two other solvent types), comparatively longer trajectories would be expected to produce a greater number of MOF-2-like square topological element in this system.

Characterization of the Self-Assembly Pathway. Across the various systems examined here, with different numbers of Zn ions and carboxylate ligands as well as different solvents, the simulations revealed several common features during the early stages of MOF self-assembly. These include multistage ordering processes characterized by different relaxation modes and formation of a mixture of transient structures featuring multiple types of topological elements. The first stage of structural evolution (corresponding to a time scale of roughly the first ~10 ns) involves the initial aggregation of Zn ions and carboxylate ligands leading to formation of 1-D chain-like structural fragments. The 1-D chain-like fragments evolve further to form generally larger and more complex (2-D or 3-D) assemblies, composed of various topological elements

during the second stage of structural evolution (occurring between ~10 and 100 ns). The vertices within these topological elements consist of different Zn-ion clusters or SBUs. During subsequent structural evolution, interconversion between different topological elements occurs within the assemblies as a third stage of the self-assembly. As the system size increases (e.g., in S_{72} and S_{200} systems), this third stage structure is manifested as a more complex and evolving conglomerate composed of different interconnected topological elements linked together in manners reminiscent of the structures observed in smaller S_8 and S_{18} systems. The third stage is a slow rearrangement process that is captured by the slowly decaying region of the PE with a relaxation time of hundreds of nanoseconds. During this third stage, the interconversion of topological elements in the system is suggestive of an apparent pseudo-steady state. It is conjectured that the fluctuation corresponding to the critical nucleus would then arise from this third stage. However, the behavior exhibited by all three model solvent systems indicates that one or two MOF-2-like square topological elements are apparently not of sufficient size to serve as a critical nucleus. Importantly, the stochastic nature of the ordering events observed during the relatively slow structural evolution can further explain why in experiments MOF-2 crystallization is a slow process. We also note that the three identified stages of structural evolution can exhibit significant temporal overlap.

Finally, it is noteworthy that the observed structural evolution in all three solvents is inconsistent with a hypothesis that assumes formation of MOFs occurring through self-assembly of preformed SBUs. To help confirm this observation, additional simulations were performed to verify the role of SBUs during the self-assembly processes in this archetypal Zn-carboxylate MOF system. The Zn ions were constrained to form pairs and trimers in two different sets of explicit DMF solvent and continuum solvent simulations, where multiple trajectories were generated for each set. In these constrained Zn-cluster systems, formation of more organized structures was observed, such as a greater number of MOF-2-like square topological elements for systems containing constrained Zn-ion pairs. However, the exclusive formation of MOF-2-like square topological elements was not seen, rather other types of topological elements such as triangular (more frequently) and five-membered rings (less frequently) also appeared. In simulation systems containing constrained Zn-ion trimers, triangular topological elements were common, consistent with a MOF-3-like structure, but other structural elements, such as square or five-membered rings and other polymeric Zn-ion structures, were also observed. These observations further support the conclusion that SBUs do not apparently play a direct role in the self-assembly of the archetypal Zn-carboxylate MOF system of interest here.

CONCLUSIONS

Using MD simulations, the current study provides important insights into the early stage mechanistic features of self-assembly for a MOF-like structure consisting of Zn ions and BDC ligands. Reproducible representative results were achieved through simulation of multiple independent trajectories where the behavior in three different solvents was compared. The influence of system size was also examined. These simulations reveal the general complexity associated with self-assembly of this archetype MOF. Self-assembly is observed to be a multistage stochastic process characterized by a variety of

transient intermediate structures. Time scales of <10, 10–100, and >100 ns were identified as key stages during the structural evolution. While the general underlying mechanism for self-assembly was similar in the three solvent systems examined, the lifetimes and probabilities of specific molecular events were observed to vary. The competing kinetic structures that emerge during the structural evolution are indicative of many local minima in the underlying free energy landscape of the system and suggest a process that achieves ordering in stages akin to systems such as proteins⁴⁵ and gas clathrate hydrates.⁴⁶ Furthermore, multistage ordering processes are also observed in other nanostructured materials. Although the presence of multiple local minima in the free energy landscape of an archetypal Zn-carboxylate system can be hypothesized (considering the multiple structures reported in the literature that can form from the combinations of Zn ions and BDC ligands), the present simulation results provide direct evidence for the same. Finally, these results provide a basis for further investigations of the nucleation and growth processes (*e.g.*, using a multiscale modeling approach) in Zn-carboxylate and similar systems characterized by complex vertex topologies. Ultimately, the insights gained would be helpful in the rational design of nanoporous materials.

METHODS

Molecular Dynamics Simulations. The MD simulations completed in this work used the GROMACS software package (4.5.5 version).⁴⁷ For the MD simulations of explicit dipolar solvent systems, initial configurations were obtained in a sol-0.8 solvent (*i.e.*, carrying charges of +0.8 and −0.8); this highly polar solvent ensured a reasonable initial solution mixture. To achieve the same in the S_{DMS8} and S_{DMF18} systems, equilibration was performed wherein the BDC and acetate ligands had carboxylic-acid-like interactions (instead of those of a carboxylate group used during the production run). For the continuum solvent S_{LD8} and S_{LD18} systems, the initial configurations were obtained by equilibrating the systems at a much higher ϵ value (*i.e.*, $\epsilon = 25$).

For all eight and 18 Zn-ion systems, multiple independent trajectories were generated to probe reproducibility and to achieve reasonable statistical averages. The simulation trajectories making up this study total to more than ~184 μ s of simulation time. Moreover, the systems were allowed to explore the configurational space freely during these simulation runs without imposing order parameter biases (*e.g.*, no additional constraints or interactions were included to regulate the self-assembly process) or exploiting unphysical simulation approaches. All production runs were performed in the NVT ensemble at a temperature of 450 K. Further simulation details are provided in the Supporting Information.

Analysis. Direct visualizations of molecular configurations from the simulation trajectories were used to analyze various structural rearrangements. To examine the time evolution of the self-assembly process, specific order parameters were evaluated, where these values focused on formation of Zn clusters and the ligand coordination of these clusters. Values were typically averaged over the set of simulation trajectories, and a single exponential smoothing technique (see the Supporting Information) was applied to time series data to help remove noise due to fluctuations.

In order to allow for appropriate interpretation in the analyses of the current simulation results, it is important to have estimates of the statistical uncertainties associated with averaged values. For example, calculations of average, minimum, and maximum values of the potential energy of system with respect to the set of independent trajectories (of that specific system) provide a measure of the distributions of the PE values (see Figure S9). Average values of cluster population typically had standard deviations of ~10–20% for all three types of solvents for the eight and 18 Zn-ion systems.

ASSOCIATED CONTENT

S Supporting Information

The Supporting Information is available free of charge on the ACS Publications website at DOI: 10.1021/acsnano.6b05444.

Details of method and models, visualization of simulation trajectories, order parameter analyses for different solvent models (PDF)

AUTHOR INFORMATION

Corresponding Author

*E-mail: pkusalik@ucalgary.ca.

ORCID

Peter G. Kusalik: 0000-0001-6270-663X

Notes

The authors declare no competing financial interest.

ACKNOWLEDGMENTS

We are grateful for the financial support of the Natural Sciences and Engineering Research Council of Canada (Grant No. RGPIN-2016-03845) and the Canadian Foundation for Innovation. We also acknowledge computational resources made available via WestGrid (www.westgrid.ca) and Compute Canada (www.computecanada.ca).

REFERENCES

- (1) Zhou, H.-C.; Kitagawa, S. Metal-Organic Frameworks (MOFs). *Chem. Soc. Rev.* **2014**, *43*, 5415–5418.
- (2) Zhou, H. – C.; Long, J. R.; Yaghi, O. M. Introduction to Metal-Organic Frameworks. *Chem. Rev.* **2012**, *112*, 673–674.
- (3) Sumida, K.; Rogow, D. L.; Mason, J. A.; McDonald, T. M.; Bloch, E. D.; Herm, Z. R.; Bae, T.-H.; Long, J. R. Carbon Dioxide Capture in Metal-Organic Frameworks. *Chem. Rev.* **2012**, *112*, 724–781.
- (4) Düren, T.; Sarkisov, L.; Yaghi, O. M.; Snurr, R. Q. Design of New Materials for Methane Storage. *Langmuir* **2004**, *20*, 2683–2689.
- (5) Suh, M. P.; Park, H. J.; Prasad, T. K.; Lim, D.-W. Hydrogen Storage in Metal-Organic Frameworks. *Chem. Rev.* **2012**, *112*, 782–835.
- (6) Brozek, C. K.; Dincă, M. Cation Exchange at the Secondary Building Units of Metal–Organic Frameworks. *Chem. Soc. Rev.* **2014**, *43*, 5456–5467.
- (7) Li, J. – R.; Sculley, J.; Zhou, H. – C. Metal–Organic Frameworks for Separations. *Chem. Rev.* **2012**, *112*, 869–932.
- (8) Herm, Z. R.; Wiers, B. M.; Mason, J. A.; van Baten, J. M.; Hudson, M. R.; Zajdel, P.; Brown, C. M.; Masciocchi, N.; Krishna, R.; Long, J. R. Separation of Hexane Isomers in a Metal-Organic Framework with Triangular Channels. *Science* **2013**, *340*, 960–964.
- (9) Liu, J.; Chen, L.; Cui, H.; Zhang, J.; Zhang, L.; Su, C. – Y. Applications of Metal–Organic Frameworks in Heterogeneous Supramolecular Catalysis. *Chem. Soc. Rev.* **2014**, *43*, 6011–6061.
- (10) Xu, R.; Wang, Y.; Duan, X.; Lu, K.; Micheroni, D.; Hu, A.; Lin, W. Nanoscale Metal-Organic Frameworks for Ratiometric Oxygen Sensing in Live Cells. *J. Am. Chem. Soc.* **2016**, *138*, 2158–2161.
- (11) Wang, C.; Zhang, T.; Lin, W. Rational Synthesis of Noncentrosymmetric Metal–Organic Frameworks for Second-Order Nonlinear Optics. *Chem. Rev.* **2012**, *112*, 1084–1104.
- (12) Kurmoo, M. Magnetic Metal–Organic Frameworks. *Chem. Soc. Rev.* **2009**, *38*, 1353–1379.
- (13) Férey, G.; Haouas, M.; Loiseau, T.; Taulelle, F. Nanoporous Solids: How Do They Form? An *In Situ* Approach. *Chem. Mater.* **2014**, *26*, 299–309.
- (14) Súrlík, S.; Millange, F.; Serre, C.; Férey, G.; Walton, R. I. An EXAFS Study of the Formation of a Nanoporous Metal–Organic Framework: Evidence for the Retention of Secondary Building Units During Synthesis. *Chem. Commun.* **2006**, *1518–1520*.

- (15) Goesten, M. G.; Stavitski, E.; Juan-Alcañiz, J.; Martínez-Joaristi, A.; Petukhov, A. V.; Kapteijn, F.; Gascon, J. Small-Angle X-ray Scattering Documents the Growth of Metal–Organic Frameworks. *Catal. Today* **2013**, *205*, 120–127.
- (16) Goesten, M. G.; Magusin, P. C. M. M.; Pidko, E. A.; Mezari, B.; Hensen, E. J. M.; Kapteijn, F.; Gascon, J. Molecular Promoting of Aluminum Metal–Organic Framework Topology MIL-101 by *N,N*-Dimethylformamide. *Inorg. Chem.* **2014**, *53*, 882–887.
- (17) Stock, N.; Biswas, S. Synthesis of Metal–Organic Frameworks (MOFs): Routes to Various MOF Topologies, Morphologies, and Composites. *Chem. Rev.* **2012**, *112*, 933–969.
- (18) Morris, R. E. How Does Your MOF Grow? *ChemPhysChem* **2009**, *10*, 327–329.
- (19) Li, M.; Dincă, M. On the Mechanism of MOF-5 Formation Under Cathodic Bias. *Chem. Mater.* **2015**, *27*, 3203–3206.
- (20) Cantu, D. C.; McGrail, B. P.; Glezakou, V.-A. Formation Mechanism of the Secondary Building Unit in a Chromium Terephthalate Metal–Organic Framework. *Chem. Mater.* **2014**, *26*, 6401–6409.
- (21) Metere, A.; Oleynikov, P.; Dzugutov, M.; O’Keeffe, M. Formation of a New Archetypal Metal–Organic Framework from a Simple Monatomic Liquid. *J. Chem. Phys.* **2014**, *141*, 234503.
- (22) Yoneya, M.; Yamaguchi, T.; Sato, S.; Fujita, M. Simulation of Metal–Ligand Self-Assembly into Spherical Complex M_6L_8 . *J. Am. Chem. Soc.* **2012**, *134*, 14401–14407.
- (23) Yoneya, M.; Tsuzuki, S.; Yamaguchi, T.; Sato, S.; Fujita, M. Coordination-Directed Self-Assembly of $M_{12}L_{24}$ Nanocage: Effects of Kinetic Trapping on the Assembly Process. *ACS Nano* **2014**, *8*, 1290–1296.
- (24) Yoneya, M.; Tsuzuki, S.; Aoyagi, M. Simulation of Metal–Organic Framework Self-Assembly. *Phys. Chem. Chem. Phys.* **2015**, *17*, 8649–8652.
- (25) Eddaoudi, M.; Moler, D. B.; Li, H. L.; Chen, B. L.; Reineke, T. M.; O’Keeffe, M.; Yaghi, O. M. Modular Chemistry: Secondary Building Units As a Basis for the Design of Highly Porous and Robust Metal–Organic Carboxylate Frameworks. *Acc. Chem. Res.* **2001**, *34*, 319–330.
- (26) Tranchemontagne, D. J.; Mendoza-Cortés, J. L.; O’Keeffe, M.; Yaghi, O. M. Secondary Building Units, Nets and Bonding in the Chemistry of Metal–Organic Frameworks. *Chem. Soc. Rev.* **2009**, *38*, 1257–1283.
- (27) Devic, T.; Serre, C. High Valence 3p and Transition Metal Based MOFs. *Chem. Soc. Rev.* **2014**, *43*, 6097–6115.
- (28) Erxleben, A. Structures and Properties of Zn (II) Coordination Polymers. *Coord. Chem. Rev.* **2003**, *246*, 203–228.
- (29) Phan, A.; Doonan, C. J.; Uribe-Romo, F. J.; Knobler, C. B.; O’Keeffe, M.; Yaghi, O. M. Synthesis, Structure, and Carbon Dioxide Capture Properties of Zeolithic Imidazolate Frameworks. *Acc. Chem. Res.* **2010**, *43*, 58–67.
- (30) Li, H.; Eddaoudi, M.; Groy, T. L.; Yaghi, O. M. Establishing Microporosity in Open Metal–Organic Frameworks: Gas Sorption Isotherms for Zn(BDC) (BDC = 1,4-Benzenedicarboxylate). *J. Am. Chem. Soc.* **1998**, *120*, 8571–8572.
- (31) Vagin, S. I.; Ott, A. K.; Rieger, B. Paddle-Wheel Zinc Carboxylate Clusters As Building Units for Metal–Organic Frameworks. *Chem. Ing. Tech.* **2007**, *79*, 767–780.
- (32) Hawxwell, S. M.; Adams, H.; Brammer, L. Two-Dimensional Metal–Organic Frameworks Containing Linear Dicarboxylates. *Acta Crystallogr., Sect. B: Struct. Sci.* **2006**, *62*, 808–814.
- (33) Yang, S. Y.; Long, L. S.; Huang, R. B.; Zheng, L. S.; Ng, S. W. Polybis(Dimethyl Sulfoxide)Zinc(II)-Di-4-Benzene-1,4-Dicarboxylato Dimethyl Sulfoxide Pentasolvate. *Acta Crystallogr., Sect. E: Struct. Rep. Online* **2005**, *61*, m1671–m1673.
- (34) Edgar, M.; Mitchell, R.; Slawin, A. M. Z.; Lightfoot, P.; Wright, P. A. Solid-State Transformations of Zinc 1,4-Benzenedicarboxylates Mediated by Hydrogen-Bond-Forming Molecules. *Chem. - Eur. J.* **2001**, *7*, 5168–5175.
- (35) Li, H.; Davis, C. E.; Groy, T. L.; Kelley, D. G.; Yaghi, O. M. Coordinatively Unsaturated Metal Centers in the Extended Porous Framework of Zn3(BDC)3,6CH3OH (BDC = 1,4-Benzenedicarboxylate). *J. Am. Chem. Soc.* **1998**, *120*, 2186–2187.
- (36) Millange, F.; Medina, I. M.; Guillou, N.; Férey, G.; Golden, K. M.; Walton, R. I. Time-Resolved *In Situ* Diffraction Study of the Solvothermal Crystallization of Some Prototypical Metal–Organic Frameworks. *Angew. Chem., Int. Ed.* **2010**, *49*, 763–766.
- (37) Guo, C.; Luo, Y.; Zhou, R.; Wei, G. Probing the Self-Assembly Mechanism of Diphenylalanine-Based Peptide Nanovesicles and Nanotubes. *ACS Nano* **2012**, *6*, 3907–3918.
- (38) Rapaport, D. C. Molecular Dynamics Simulation of Reversibly Self-Assembling Shells in Solution Using Trapezoidal Particles. *Phys. Rev. E* **2012**, *86*, 051917.
- (39) Cauët, E.; Bogatko, S.; Weare, J. H.; Fulton, J. L.; Schenter, G. K.; Bylaska, E. J. Structure and Dynamics of the Hydration Shells of the Zn(2+) Ion From *Ab initio* Molecular Dynamics and Combined *Ab initio* and Classical Molecular Dynamics Simulations. *J. Chem. Phys.* **2010**, *132*, 194502.
- (40) Inada, Y.; Hayashi, H.; Sugimoto, K. – I.; Funahashi, S. Solvation Structures of Manganese(II), Iron(II), Cobalt(II), Nickel(II), Copper(II), Zinc(II), and Gallium(III) Ions in Methanol, Ethanol, Dimethyl Sulfoxide, and Trimethyl Phosphate As Studied by EXAFS and Electronic Spectroscopies. *J. Phys. Chem. A* **1999**, *103*, 1401–1406.
- (41) Ye, B. – H.; Li, X. – Y.; Williams, H. D.; Chen, X. – M. Synthesis and Structural Characterization of Di- and Tetranuclear Zinc Complexes with Phenolate and Carboxylate Bridges. Correlations between ¹³C NMR Chemical Shifts and Carboxylate Binding Modes. *Inorg. Chem.* **2002**, *41*, 6426–6431.
- (42) Williams, C. A.; Blake, A. J.; Hubberstey, P.; Schröder, M. A. Unique Example of a 3⁶ Tessellated 2-D Net Based on a Tri-Nuclear Zinc(II)-1,4-Benzenedicarboxylate Framework. *Chem. Commun.* **2005**, *5435*–5437.
- (43) Dincă, M.; Long, J. R. Strong H₂ Binding and Selective Gas Adsorption within the Microporous Coordination Solid Mg₃(O₂C₁₀H₅CO₂)₃. *J. Am. Chem. Soc.* **2005**, *127*, 9376–9377.
- (44) Banerjee, D.; Parise, J. B. Recent Advances in s-Block Metal Carboxylate Networks. *Cryst. Growth Des.* **2011**, *11*, 4704–4720.
- (45) Dill, K. A.; Chan, H. S. From Levinthal to Pathways to Funnels. *Nat. Struct. Biol.* **1997**, *4*, 10–19.
- (46) Vatamanu, J.; Kusalik, P. G. Observation of Two-Step Nucleation in Methane Hydrates. *Phys. Chem. Chem. Phys.* **2010**, *12*, 15065–15072.
- (47) Pronk, S.; Páll, S.; Schulz, R.; Larsson, P.; Bjelkmar, P.; Apostolov, R.; Shirts, M. R.; Smith, J. C.; Kasson, P. M.; van der Spoel, D.; Hess, B.; Lindahl, E. GROMACS 4.5: A High-Throughput and Highly Parallel Open Source Molecular Simulation Toolkit. *Bioinformatics* **2013**, *29*, 845–854.